New Petroleum Absorbers Based on Lignin-CNSL-Formol Magnetic Nanocomposites

E. G. O. Grance,[1] F. G. Souza, Jr.,[1] A. Varela,[1] E. D. Pereira,[1] G. E. Oliveira,[2] C. H. M. Rodrigues[3]

[1]*Laboratório de Biopolímeros e Sensores, Instituto de Macromoléculas, Universidade Federal do Rio de Janeiro, Centro de Tecnologia, Bloco J, Ilha do Fundão, Rio de Janeiro, RJ 21941-914, Brazil*
[2]*Departamento de Química/Centro de Ciências Exatas, Universidade Federal do Espírito Santo Av. Fernando Ferrari, s/n, Goiabeiras, Vitória, ES 29075-910, Brazil*
[3]*Instituto Federal do Espírito Santo (IFES), Unidade de Aracruz/ES, Av. Morobá S/N, Morobá, Aracruz ES, 29199-000, Brazil*

Received 20 May 2011; accepted 9 February 2012
DOI 10.1002/app.36998
Published online in Wiley Online Library (wileyonlinelibrary.com).

ABSTRACT: A magnetic resin based on lignin produced using the Kraft process was prepared and characterized. The material, because of its aromatic/aliphatic balance, can be used in oil-spill clean-up processes. The resin was prepared through bulk polycondensation of lignin, cashew nutshell liquid, and formaldehyde in the presence of maghemite nanoparticles. The obtained magnetic composites were studied by Fourier transform infrared spectroscopy, X-ray diffraction, and Small-angle X-ray scattering. Cure degree, magnetic force, and oil removal capability tests were also performed. The results show that the composites possess an elevated cure degree, besides a considerable magnetic force. The materials exhibit a good oil removal capability—the composite containing 3.3 vol % of maghemite can remove 11 parts of oil from water. © 2012 Wiley Periodicals, Inc. J Appl Polym Sci 000: 000–000, 2012

Key words: environmental recovery; oil spill cleanup; lignin; CNSL; maghemite; magnetic nanocomposites

INTRODUCTION

Petroleum is largely consumed by human kind and the largest amount of this nonrenewable resource is transported by marine routes. Unfortunately, accidents involving petroleum spill are very ordinary and the estimated amount of the spilled oil around the world is equal to 400,000 tons per year.[1] These spills produce severe impacts on the environment, being directly responsible for the destruction of the marine life, since the lipophilic hydrocarbons interaction with lipid layers of flora and fauna causes intoxication and even death. In addition, spills are also able to impact the food and even the tourism industries.

Among the traditional oil spill cleanup processes, the most used are (i) the natural dispersion; (ii) the containment and skimming; (iii) the *in situ* burning; (iv) the use of sorbents; and (v) the use of detergents and dispersants. The last one, as seen in Torrey Canyon (1967)[1] and Alaska (1989)[2,3] spills, was not effective and also contributed for increasing the amount of toxic elements in the environment, making harder the bio-recovery of the ecosystem. The devastation extension caused by accidents, as in Dalian/China (2010), Gulf of Mexico (2010), as well as in Campos/Brazil (2011), shows that new strategies of remediation must be continuously studied. In this specific context, our group is focused on the use of renewable resources able to be transformed in polymer materials useful to the absorption of petroleum from the water.[4–7] Among these renewable resources, good absorption results are provided by resins prepared using the cashew nutshell liquid and lignin from Kraft process. Cashew nutshell liquid (CNSL) is an important by-product of the cashew nut industry. The potential annual availability of this material, which accounts for about 32 wt % of the cashew shell, is enormous. Industrial application of CNSL-based products are numerous, including phenolic resins,[8] brake linings, paints and primers, foundry chemicals, lacquers, cements, coatings, and transformed cardanol for gasoline stabilization.[9] The main component of CNSL is cardanol, a phenol derivative that presents a C15 unsaturated hydrocarbon chain with 1–3 double bonds in the meta position.[10–13] Because of its structure, cardanol

Correspondence to: F. G. Souza, (fgsj@ufrj.br).

The authors thank to Conselho Nacional de Desenvolvimento Científico e Tecnológico (CNPq), Coordenação de Aperfeiçoamento de Pessoal de Nível Superior (CAPES-NANOBIOTEC) and Fundação Carlos Chagas Filho de Amparo à Pesquisa do Estado do Rio de Janeiro (FAPERJ) for the financial support and scholarships. The authors also thank to Brazilian Synchrotron Light Laboratory (LNLS) by support on AFM (LNLS, Brazil-AFM/9637/10) and SAXS experiments (D11A-SAXS1-9077, SAXS1-9078 and D11A-SAXS1-11596).

can also be used as a stabilizer of liquid–liquid dispersions and/or a plasticizer.

Lignin is a complex hydrocarbon polymer with both aliphatic and aromatic constituents.[14–16] These macromolecules posses a polyphenolic nature with low toxicity and it can be used as a total or partial substitute for phenol in the formulation of phenolic resins.[17] Beyond largely available—world's production is around 30 million tons per year[18]—the complex structure of lignin is very interesting since it can be useful to tuning aromatic/aliphatic balance in resins, making them better petroleum absorbers. From the environmental point of view, this strategy is interesting because it avoids the use of nonrenewable materials inside impacted areas.

Aiming to make easier the cleanup process, the green resins can be prepared in the presence of magnetic nanoparticles based on iron oxides, which are ecologically appropriated and easily produced.[4] Among magnetic nanoparticles, the maghemite is largely studied[19,20] since it possesses strong magnetic force associated with a superparamagnetic behavior.[4–7] The produced materials were characterized using Fourier transform infrared spectroscopy (FTIR), X-ray diffraction (XRD), and Small-angle X-ray scattering (SAXS). In addition, the magnetic force, the oil removal capability, and the residual oil were also analyzed.

EXPERIMENTAL

Materials

Cobalt (II) chloride hexahydride ($CoCl_2.6H_2O$), ferric chloride ($FeCl_3$), anhydrous sodium sulfite (Na_2SO_3), and ammonium hydroxide (NH_4OH) were purchased from Vetec/Brazil as analytical grades. Hydrochloric acid (HCl) was purchased from Proquímica/Brazil as analytical grade. These reagents were used for preparation of maghemite particles as received, without further purification.

Cashew nutshell liquid (CNSL) was kindly supplied by RESIBRAS-Brazil. The lignin was kindly provided by *KLABIN* (Rio de Janeiro, Brazil). This lignin presented M_w and M_n equal to 2351 g/mol and 1396 g/mol, respectively. Furfural and sulfuric acid were purchased from Vetec/Brazil as analytical grades. These reagents were used for preparation of the resins as received, without further purification.

Synthesis of maghemite particles

The syntheses of the maghemite particles were performed as described in the literature.[4,5,21] Initially, aqueous solutions of hydrochloric acid (2*M*), ferric chloride (2*M*), and sodium sulfite (1*M*) were prepared. In a typical procedure, 30 mL of the ferric chloride solution and 30 mL of deionized water were added into a beaker under continuous agitation. Soon afterwards, 20 mL of the sodium sulfite solution was added to the beaker, also under continuous agitation. The reaction product was precipitated by slowly adding 51 mL of concentrated ammonium hydroxide into the beaker under continuous agitation. After 30 min, the medium was filtrated and the obtained particles were washed several times with water and finally dried at 60°C in an oven. Magnetite was converted into maghemite through annealing at 200°C for 1 h.

Polymerization and preparation of the composite

CNSL, lignin, and formaldehyde resins were prepared through acid catalysis. Lignin (1 phr), CNSL (1.5 phr), and formaldehyde (3.2 phr) were poured into a three-necked flask under continuous stirring. Medium was warmed at 75°C. Soon afterwards, medium was acidified using acetic acid (0.2 phr) and stirring was kept until the formation of a solid material. Composites were prepared following a procedure similar to the one described to the resin preparation. In these cases, maghemite was inserted before acidification in two different amounts equal to 0.7 and 3.3 vol % of the maghemite inside composites, respectively.

Characterization

Atomic force microscopy (AFM) was used for determination of the characteristic diameter of the produced maghemite particles. AFM was performed in a DI Nanoscope IIIa microscope (LNLS, Brazil—AFM/9637/10), at non-contact mode, NSC-10-50, 20 N m^{-1} and 260 kHz. Image Analysis3.5 software was used to the tip deconvolution process using the following parameters: Single crystal silicon, N-type, 0.01–0.025 Ohm cm, antimony doped produced by NT-MDT with pyramid tip, cantilever length 125 ± 10 μm. Soon afterwards, 30 particles were randomly chosen to perform diameter calculations.

FTIR analyses were performed in a Nicolet iN10 Spectrometer, using a MCT-B detector and a diffuse reflectance accessory, resolution equal to 4 cm^{-1} and accumulation along 24 scans.

Wide-angle X-ray scattering (WAXS)/SAXS measurements were performed with the beamline of the Brazilian Synchrotron Light Laboratory (LNLS, Brazil D11A—SAXS1-9077). This beam line is equipped with an asymmetrically cut and bent silicon (111) monochromator ($\lambda = 1.7556$ Å), which yields a horizontally focused X-ray beam. A linear position-sensitive X-ray detector (PSD) and a multichannel analyzer were used to determine the SAXS intensity $I(q)$ as function of the modulus of the scattering vector $q = (4\pi/\lambda) \sin \theta$, 2θ being the scattering angle. All SAXS spectra were corrected for the parasitic

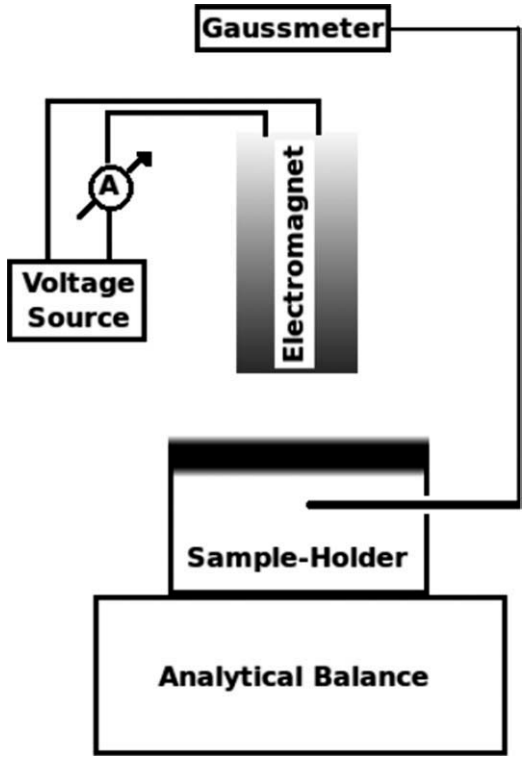

Figure 1 Experimental setup used in magnetic force versus magnetic field tests.

scattering intensity produced by the collimating slits, for the non-constant sensitivity of the PSD, for the time varying intensity of the direct synchrotron beam, and for differences in sample thickness. Thus, the SAXS intensity was determined for all samples in the same arbitrary units, so that they can be directly compared to each other. Since the incident beam cross-section at the detection plane is small, no mathematical deconvolution of the experimental SAXS function was needed.[22,23]

Cure degree was determined through extraction method, using toluene as solvent. The permanence time inside the Soxhlet extractor was equal to 20 h.

Flotation capability tests were performed in water and in ethanol. In each case, 1 g of the resin was poured on the liquid surface. After 5 min, a visual inspection was performed and qualitative results were registered.

Magnetic force was determined with the help of a simple experimental setup, showed in Figure 1. This setup is constituted by an analytical balance Shimadzu AY-220, a voltage source ICEL PS-4100, a digital multimeter ICEL MD-6450, a Gaussmeter GlobalMag TLMP-Hall-02; a home-made sample holder and a home-made electromagnet. System calibration was performed in the absence of magnetic material. First, using the ampermeter and the gaussmeter, a current versus magnetic field calibration was performed. Soon afterwards a current versus mass calibration was also performed. Obtained results were used to predict part of the presented error. Magnetic force tests were performed following the mass variation of the sample in the presence of different magnetic field, produced by the electromagnet. Then, the apparent variation of mass of the sample in the presence of magnetic field was calculated subtracting the mass of the sample in the presence of magnetic field from the mass of sample. The magnetic force (opposite to gravitational one) was calculated according to eq. (1).

$$F_m = \Delta m g \tag{1}$$

where F_m is the magnetic force, Δm is the apparent variation of mass in the presence of the magnetic field, and g is the acceleration of gravity. As reference, the magnetic force of a cobalt (II) chloride hexahydride standard sample was calculated according to this method and obtained result is equal to (0.18 $\pm$ 0.02) mN at (838 $\pm$ 1) Gauss.

The oil removal tests (GOr) were performed according to the analytical procedure established in our laboratory,[4–7] comprising the following steps:

1. Approximately 1 g of the magnetic composite is weighed (m_1).

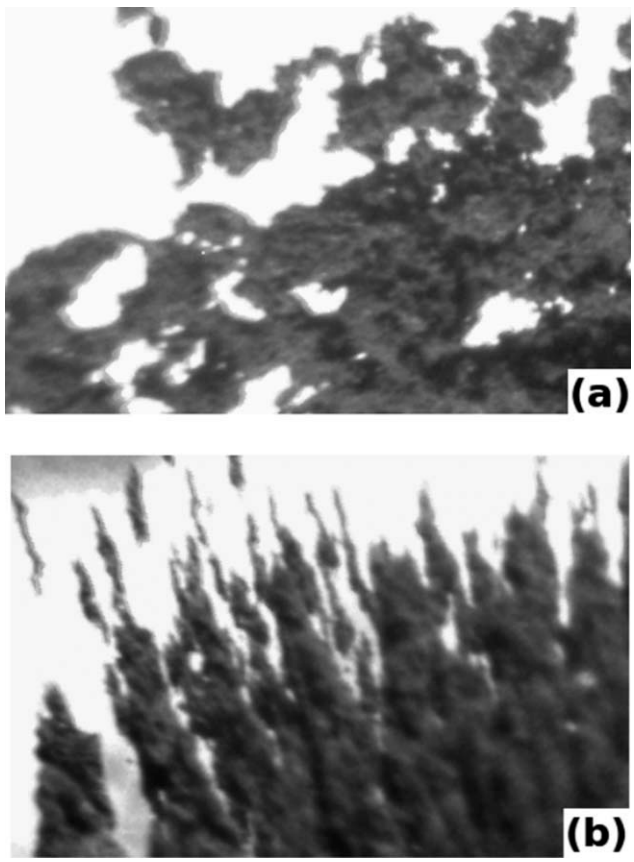

Figure 2 Maghemite in the presence of external magnetic field—"off" (a) and "on" (b) ×25.

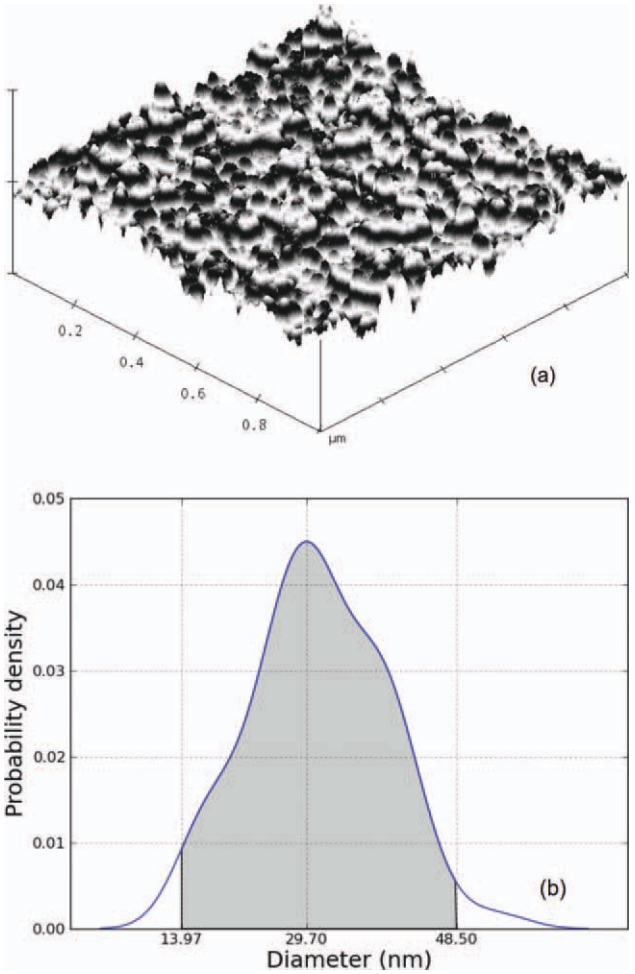

Figure 3 AFM of maghemite (a) and respective diameter distribution of the particles (b). [Color figure can be viewed in the online issue, which is available at wileyonlinelibrary.com.]

2. 90 mL of water is poured into a beaker and the total mass is determined.
3. A known mass of the oil (m_2) is spilt on the water.

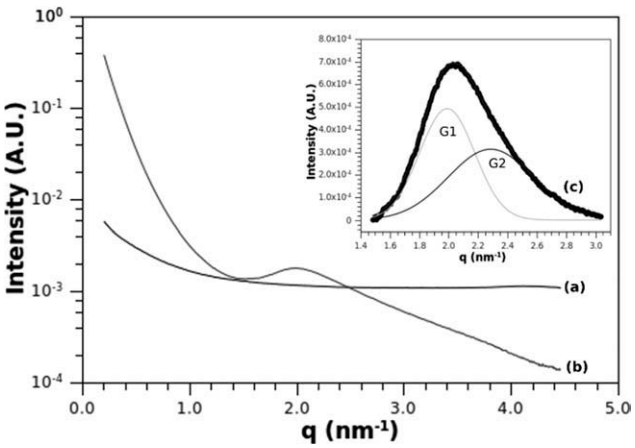

Figure 4 SAXS of the resin (a) and composite containing 0.7 vol % of maghemite (b). Distance distribution function obtained from SAXS is shown inset (c).

TABLE I
Flotation Capability (FC), Density, and Cure Degree of the Materials

Maghemite (vol %)	FC (water)	FC (ethanol)	Density (g/cm^3)[a]	Cure degree (%)
0.0	+	−	0.83 ± 0.01	94 ± 5
0.7	+	−	0.85 ± 0.02	94 ± 4
3.3	+	−	0.93 ± 0.01	93 ± 5

[a] Tests performed in ethanol, $d = 0.7800$ g/mL at 20°C.

4. The magnetic composite is added into the beaker (containing the water and the oil).
5. After 5 min the oil and composite are magnetically removed.
6. The mass of the oil residue is determined (m_3).
7. Gravimetric oil removal is calculated according to eq. (2).

$$\mathrm{OR} = \frac{m_2 - m_3}{m_1} \quad (2)$$

Weighing was carried out with the help of analytical balances.

RESULTS AND DISCUSSION

Optical microscopy under magnetic field provides a simple and important characterization tool for the magnetic particles. Figure 2 shows that the presence of the magnetic field produces an alignment of the maghemite particles, which is immediately lost when magnetic field is removed. This behavior indicates that produced maghemite possesses an intrinsic magnetism, allowing their use to magnetic composite preparation.

AFM micrograph of pure maghemite particles is shown in Figure 3. The obtained particle size

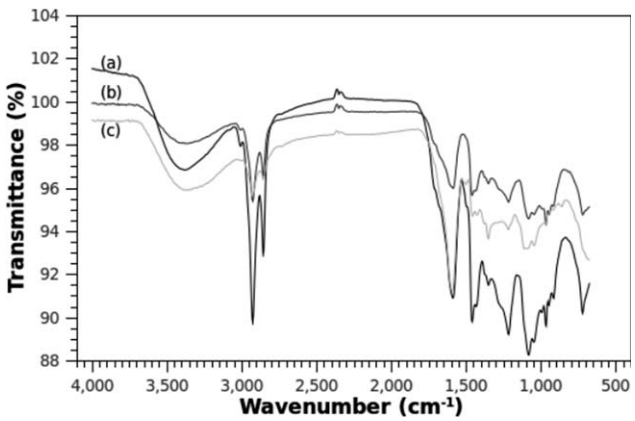

Figure 5 FTIR of resin (a), and composites containing 0.7 vol % (b) and 3.3 vol % (c) of maghemite.

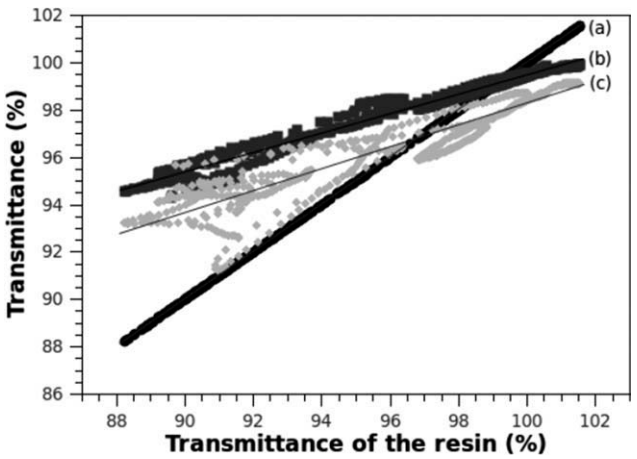

Figure 6 Statistical analysis of FTIR spectra of resin (a), and composites containing 0.7 vol % (b) and 3.3 vol % (c) of maghemite.

distribution of the maghemite particles is also shown in the same figure. According to this figure, maghemite particles present spherical morphology and low degree of aggregation. Particle diameters were calculated with the Image Analysis software,[24] while particle size distributions were computed as described in other work of our group.[25,26] Figure 3 shows that particle diameter distributions present a single mode, is narrow and asymmetric, concentrating 95% of the particles in the range 23^{+8}_{-5} nm. In addition, the presented probability density function could be split in two Gaussian functions [see inset of the Fig. 3(b)]. These functions are related with the existence of two main diameters of the nanoparticles equal to 23 ± 3 nm and 29 ± 2 nm, respectively.

Particle size of the nanoparticles in the composite was also investigated using SAXS. Figure 4 shows SAXS profiles for the resin (a) and composite containing 0.7 vol % of maghemite. SAXS profile of the composite presents a broad correlation full-width at half-maximum (FWHM) peak in the 1.4–2.5 nm^{-1} range. Baseline subtraction and peak deconvolution (see inset of the Fig. 4) were performed before data analyses. The shape of the curve and the higher correlation ($R^2 = 0.9990$) between experimental data and the model composed of two gaussians indicate the existence of distinct nanometric spatial heterogeneities.[23,27] The average and most probable distance d_S between spatial heterogeneities can be estimated as[28]:

$$d_S = 2\pi/q_{\max} \quad (3)$$

where $q_{\max}$ is the modulus of the scattering vector at the peak maximum. The presence of the reported X-ray scattering phenomenon in composite is due to the existence of ordered nanometric crystalline regions (heterogeneities), composed by maghemite and its superstructures, dispersed in a mostly amorphous matrix.[22,23]

The average size of the spatial heterogeneities (which provides an estimate for the disordered "supercrystal" size), L_C, can be obtained as[27]:

$$L_C = 4\pi/\Delta q \quad (4)$$

where Δq is the FWHM of the peak.

For the composite, L_C values for peaks placed at 1.99 nm^{-1} and 2.29 nm^{-1} are respectively equal to 28 ± 3 nm and 18 ± 2 nm, respectively, indicating that distinct maghemite superstructures may exist. The average distance among crystals, d_S, as calculated with eq. (3) is equal to 3.2 ± 0.3 nm and 2.7 ± 0.3 nm, respectively. Values obtained from AFM and SAXS are in complete agreement, indicating the obtaining of magnetic nanoparticles.

Density, flotation capability (FC), and cure degree of the resin and composites were also studied. Obtained results are shown in Table I.

FC tests were performed using water and ethanol. Resin and composites were able to float on the water. The same behavior was not observed when ethanol was used. Therefore, qualitative test used is encouraging since showed that magnetic composites possess density values lower than the one of the water.

Density of the materials is also shown in Table I. Materials containing 0.0, 0.7, and 3.3 vol % of maghemite presented densities equal to 0.83 ± 0.01 g/cm^3; 0.85 ± 0.02 g/cm^3, and 0.93 ± 0.01 g/cm^3, respectively. All the obtained values guarantee the good fluctuation of the composites. In addition, results showed, with a correlation equal to 0.9998, that density of composites is linearly related with volumetric amount of the maghemite. This kind of

TABLE II
Correlation and Root Mean Squared Error Between Transmittances of the Composites and Pure Resin

Maghemite (vol %)	Linear coefficient	Angular coefficient	R^2	RMSE[a]
0.0	$(0.00 \pm 0.00) \times 10^0$	$(1.00 \pm 0.00) \times 10^0$	1.0000	0.00
0.7	$(5.85 \pm 0.02) \times 10^1$	$(4.10 \pm 0.02) \times 10^{-1}$	0.9792	0.23
3.3	$(5.19 \pm 0.05) \times 10^1$	$(4.64 \pm 0.05) \times 10^{-1}$	0.8936	0.62

[a] Root mean squared error.

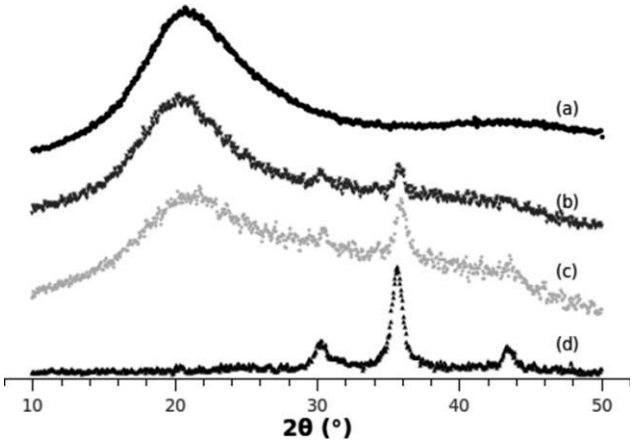

Figure 7 DRX of the resin (a); composites containing 0.7 (b), 3.3 vol % (c) of maghemite and pure maghemite (d).

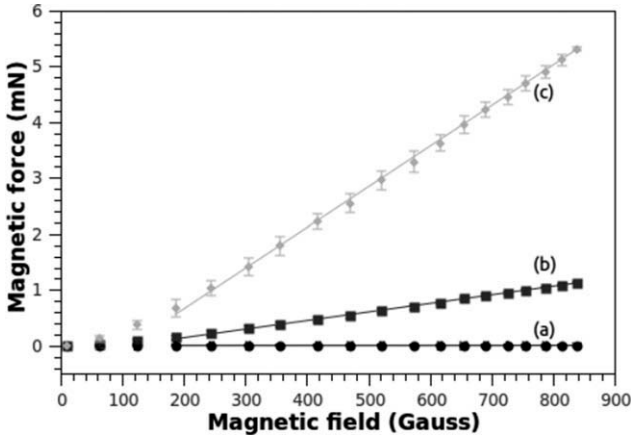

Figure 8 Magnetic force versus magnetic field of the resin (a); and composites containing 0.7 (b) and 3.3 vol % (c) of maghemite.

behavior agrees with the classical linear law of the mixtures.[29] As density values are lower than the one of the water, these results are also in complete agreement with flotation ones.

Cure degree results are also presented in Table I. The obtained values were statistically the same and the average cure degree was equal to (94 ± 5)%. This is an interesting result since the resin is insoluble in ordinary organic solvents, which means that petroleum may be extracted from the absorber by the use of a washing process.

FTIR-Attenuated total reflectance spectra of the pure resin and its composites are shown in Figure 5. Resin presents a typical phenol/formaldehyde resin FTIR spectrum. This spectrum indicates that polymerization reactions occurred in the aromatic ring and that the unsaturated aliphatic chains are preserved. The characteristic bands present in the spectrum of the resin are: a wide band at 3325 cm^{-1} related to stretching of OH present in phenol and FeOH. The small characteristic band placed at 2958 cm^{-1} corresponds to stretching of C—H and the doublet at 2920 cm^{-1} and 2850 cm^{-1} is related to stretching of CH_2 and CH_3. The characteristic band at 1589 cm^{-1} is related to aliphatic C=C stretching. The doublet at 1450 cm^{-1} and 1419 cm^{-1} is characteristic of the C=C stretching of the aromatic ring. The band at 1207 cm^{-1} corresponds to C—O—C asymmetric stretching and symmetric stretching of this bond appears at 1068 and 1034 cm^{-1}. The characteristic band at 1168 cm^{-1} is O—C—C stretching together with 1034 cm^{-1}. Therefore, these two bands represent conjugated vibrations of the C—O—C and O—C—C groups. The band at 960 cm^{-1} is characteristic of the asymmetric stretching of C=C bond in aromatic rings. The band placed at 714 cm^{-1} is characteristic of asymmetric stretching of aliphatic CH_2. Comparing the spectrum of the pure resin with the spectrum of the composites, no significant differences can be observed in the main bands, probably indicating the absence of significant chemical interactions between the matrix and the filler.[26,30,31] However, other changes in spectra could be detected by statistical analysis, shown in Figure 6 and in Table II. Figure 6 shows the transmittance of the pure resin and its composites versus the transmittance of the pure resin. Figure 6 shows clearly that the increase of maghemite amount leads to an increase of the dispersion of the data. Furthermore, the comparison between data of the resin and composites shown in Table II indicates that the increase of the maghemite amount in the composites leads to a decrease of the correlation and an increase of the root mean squared error (RMSE). The increase of the RMSE is related to an increase of the misfit between experimental data and model.[32] These results could be useful to perform further correlations about the maghemite amount in the composites.

Figure 7 presents the WAXS patterns of the maghemite, resin, and composites. Resin presented a typical amorphous pattern while the pure maghemite presented peaks at 20.4°, 30.4°, 36.2°, and 43.5°. According to Millan et al.,[33] these peaks correspond to (111), (220), (311), and (400) reflections of a spinel crystal structure such as presented by maghemite or magnetite.

TABLE III
Crystal Size and Crystallinity Degree of the Analyzed Materials

Maghemite (vol %)	Crystallinity degree (%)	CS (nm)[a]	R^2
0	6.1 ± 0.4	–	–
0.7	10.8 ± 0.3	19 ± 2	0.9858
3.3	17.5 ± 0.9	15 ± 1	0.9995
100	76 ± 2	17 ± 2	0.9884

[a] Crystal size calculated at (311) peaks using Scherrer equation [eq. (3)].

TABLE IV
Linear Models of Magnetic Force Versus Magnetic Field

Maghemite (vol %)	Linear coefficient	Angular coefficient	R^2	RMSE[a]
0.0	$(0.30 \pm 8.42) \times 10^{-3}$	$(0.19 \pm 1.79) \times 10^{-6}$	0.4489	0.04
0.7	$(1.7 \pm 0.2) \times 10^{-1}$	$(1.54 \pm 0.03) \times 10^{-3}$	0.9998	0.34
3.3	$(8.0 \pm 0.9) \times 10^{-1}$	$(7.3 \pm 0.1) \times 10^{-3}$	0.9997	0.35

[a] Root mean squared error.

Crystallinity degree was calculated according Ruland's method[34] while crystal sizes were calculated with the Scherer's equation [eq. (5)][26] and presented in Table III.

$$\mathrm{CS} = \frac{k\lambda}{\Delta\theta \cos\theta} \quad (5)$$

In eq. (5), K is a constant (equal to 1.0), λ is the wavelength, θ is the Bragg angle ($2\theta/2$), and $\Delta\theta$ is the FWHM of the (311) peaks. Pure maghemite presented crystallinity degree and crystal size equal to (76 ± 2)% and (17 ± 2) nm, respectively. The crystal size was calculated with a R^2 equal to 0.9884. Other produced composites, containing 0.7 vol % and 3.3 vol %, presented crystal sizes of 19 ± 2 nm and 15 ± 2 nm (see Table III), indicating that the crystalline structure of the filler inside the composites remained essentially the same. These values are similar to the ones reported in other works of the group where maghemite inside polymer matrix presented crystalline size equal to 19 ± 1 nm[4] and 21 ± 2 nm.[5] The obtained results indicate that the maghemite properties are probably preserved in the hybrids. In addition, as expected, the increase of the maghemite content leads to the increase of the degree of crystallinity and raising of the characteristic diffraction peaks of the pure maghemite (see Table III and Fig. 7).

The magnetic force of the composites was also studied. Obtained results are shown in Figure 8. Linear fit was performed on each curve of the Figure 8. These models were calculated in range 187–838 Gauss and results are showed in Table IV.

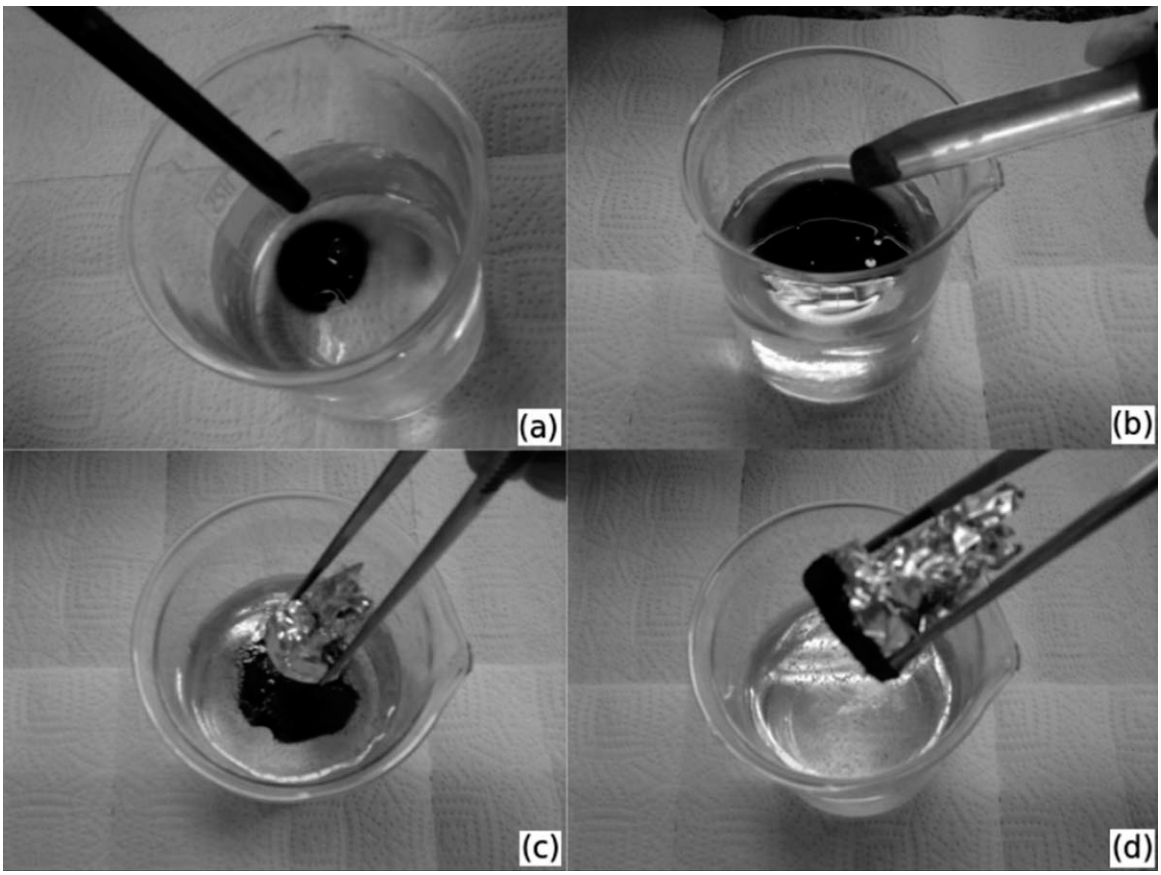

Figure 9 Oil spill cleanup using composite containing 3.3 vol % of maghemite. Spill of the oil (a); insertion of the composite (b); magnet close to mixture (c) and final cleanup (d).

Composites presented good correlations and RMSE quite similar. Angular coefficients of the composites are proportional to the maghemite volume amount in the composites. In addition, magnetic force at maximum magnetic field (equal to 838 ± 1 Gauss) of the composites containing 0.7 and 3.3 vol % of maghemite were equal to (1.08 ± 0.01) mN and (5.1 ± 0.1) mN, respectively. These values are significantly lower than the one for the pure maghemite, equal to (355 ± 7) mN and only the composite containing 3.3 vol % of maghemite presented magnetic force able to make it useful in oil removal tests (see Fig. 9). These results are presented as grams of the oil removed by each gram of the composite. Thus, these results are dimensionless. Composite containing 3.3 vol % of maghemite presented oil removal capability equal to (11.2 ± 0.5) g/g. Thus, each gram of the resin is able to remove around 11 g of the petroleum from the water. Therefore, this is a very encouraging result, since in other works of our group,[4,5] magnetic composites based on polyurethanes and alkyd resins were able to remove (4.1 ± 0.1) g/g[5] and (8.33 ± 0.19) g/g[4] of petroleum, respectively.

CONCLUSIONS

Main objective of this work was achieved since lignin-CNSL-formol/maghemite composite was able to present a good combination of magnetic properties with oil removal capability. In addition, AFM and SAXS results showed the obtaining of nanomaterials. Obtained composites presented a density lower than that of water, allowing their easy flotation. Each gram of the composite was able to remove around 11 g of the petroleum from the water. These materials also presented an expressive cure degree, equal to (94 ± 5)%, making them able to pass through a solvent bath, useful in future oil recovery processes. Therefore, the prepared material contributes to the environment encouraging nobler uses to some of the available renewable resources besides reducing the environmental anthropogenic impact on areas degraded by oil spill accidents.

References

1. Coleman, J.; Baker, J.; Cooper, C.; Fingas, M.; Hunt, G.; Kvenvolden, K.; Michel, K.; Michel, J.; Mcdowell, J.; Phinney, J.; Pond, R.; Rabalais, R.; Roesner, L.; Spies, R.B. Oil in the Sea III: Inputs, Fates, and Effects. The National Academies Press, Washington, D.C., 2003, p 16.
2. Bellamy, D. J.; Clarke, P. H.; John, D. M.; Jones, D.; Whittick, A.; Darke, T. Nature 1967, 216, 1170.
3. Bragg, J. R.; Prince, R. C.; Harner, E. J.; Atlas, R. M. Nature 1994, 368, 413.
4. Souza, F. G., Jr.; Marins, J. A.; Rodrigues, C. H. M.; Pinto, J. C. Macromol Mater Eng 2010, 295, 942.
5. Lopes, M. C.; Souza, F. G., Jr.; Oliveira, G. E. Polímeros 2010, 20, 359.
6. Souza, F. G., Jr.; Oliveira, G. E.; Lopes, M. Invited talk in the Second International Conference on Natural Polymers; India, 2010. Available from http://www.biopolymers.macromol.in/abstracts/fernandogomes.pdf; Accessed on 5 Feb. 2011.
7. Oliveira, G. E.; Souza, F.G., Jr.; Lopes, M. Invited talk in the Second International Conference on Natural Polymers; India, 2010. Available from http://www.biopolymers.macromol.in/abstracts/geizaesperandiodeoliveira.pdf; Accessed on 05 Feb. 2011. (2010).
8. Yadav, R.; Devi, A.; Tripathi, G.; Srivastava, D.; Eur Polym J 2007, 43, 3531.
9. Mathew, G.; Rhee, J. M.; Hwang B. S.; Nah, C. J Appl Polym Sci 2007, 106, 178.
10. Arayapranee, W.; Rempel, G. L. J Appl Polym Sci 2007, 106, 2696.
11. Souza, F. G., Jr.; Pinto, J. C.; Soares, B. G. Eur Polym J 2007, 43, 2007.
12. Mohapatra, D. K.; Das, D.; Nayak, P. L.; Lenka, S. J Appl Polym Sci 1998, 70, 837.
13. Souza, F. G., Jr.; Orlando, M. T. D.; Michel, R. C.; Pinto, J. C.; Cosme, T.; Oliveira, G. E. J Appl Polym Sci 2011, 119, 2666.
14. Johna, M. J.; Thomas, S. Carbohydr Polym 2008, 71, 343.
15. Botros, S. H.; Eid, M. A. M.; Nageeb, Z. A. J Appl Polym Sci 2006, 99, 2504.
16. Xu, F.; Sun, R.-C.; Zhai, M.-Z.; Sun, J.-X.; Jiang, J.-X.; Zhao, G.-J. J Appl Polym Sci 2008, 108, 1158.
17. Vazquez, G.; Rodriguez, B.C.; Freire, S.; Gonzalez, A. J.; Antorrena, G. Bioresource Technol 1999, 70, 209.
18. Hatakeyama, T.; Hatakeyama, H. Thermal Properties of Green Polymers and Biocomposites; Kluer Academic Publishers: New York, 2004; p 7.
19. Govindaraj, B.; Sastry, N. V.; Venkataraman, A. J Appl Polym Sci. 2004, 93, 778.
20. Faridi-Majidi, R.; Sharifi-Sanjani, N. J Appl Polym Sci 2007, 105, 1351.
21. Souza, F. G., Jr.; Marins, J. A.; Pinto, J. C.; Oliveira, G. E.; Rodrigues, C. H. M. J Mater Sci ICAM 2009 2010, Special Issue, 4231.
22. Souza, F. G., Jr.; Oliveira, G. E.; Rodrigues, C. H. M.; Soares, B. G.; Nele, M.; Pinto, J. C. Macromol Mater Eng 2009, 294, 484.
23. Souza, F. G., Jr.; Soares, B. G.; Dahmouche, K. J Polym Sci Part B Polym Phys 2007, 45, 3069.
24. Image Processing and Analysis in Java. Software available in site http://rsbweb.nih.gov/ij.
25. Souza, F. G., Jr.; Soares, B. G.; Pinto, J. C. Eur Polym J 2008, 44, 3908.
26. Souza, F. G., Jr.; Richa, P.; Siervo, A.; Oliveira, G. E.; Rodrigues, C. H. M.; Nele, M.; Pinto, J. C. Macromol Mater Eng 2008, 293, 675.
27. Glatter, O.; Kratky, O. Small-Angle X-ray Scattering; Academic Press: New-York, 1982.
28. Berner, D.; Travers, J. P.; Rannou, P. Synth Met 1999, 101, 836.
29. Fan, Z.; Miodownik, A. P. J Mater Sci 1994, 29, 141.
30. Souza, F. G., Jr.; Pinto, J. C.; Rodrigues, M. V.; Anzai, T. K.; Richa, P.; Melo, P. A.; Nele, M.; Oliveira, G. E.; Soares, B. G. Polym Eng Sci 2008, 48, 1947.
31. Raiskila, S.; Pulkkinen, M.; Laakso, T.; Fagerstedt, K.; Löija, M.; Mahlberg, R.; Paajanen, L.; Ritschkoff, A.-C.; Saranpää, P. Silva Fennica 2007, 41, 351.
32. Kelley, K.; Lai, K. Multivariate Behav Res 2011, 46, 1.
33. Millan, A.; Palacio, F.; Falqui, A.; Snoeck, E.; Serin, V.; Bhattacharjee, A.; Ksenofontov, V.; Gutlich, P.; Gilbert, I. Acta Mater 2007, 55, 2201.
34. Ruland, W. Acta Cryst 1961, 14, 118.